# The solar Total Irradiance Monitor: TIM

*George M. Lawrence, Gary Rottman, Jerald Harder, Thomas Woods Laboratory for Atmospheric and Space Physics, University of Colorado, Boulder, CO 80309-0590, U.S.A.*

**Abstract.**

Launching in 2002 on the EOS SORCE (Solar Radiation and Climate Experiment), TIM is an active cavity radiometer that will point at the Sun on orbit, and monitor the total solar irradiance. The accuracy will be better than 100 ppm (1 $\sigma$) with a noise level < 1 ppm each 500 seconds. Sunlight passes through a shutter, a 50 $mm^2$ aperture, a baffle section; and then is absorbed into a 14 g silver cavity blackened inside with Nickel Phosphorous (NiP). Embedded in the walls of the cavities are electrical substitution heaters. Diamond electrical terminals help localize thermal nodes. Four cavities align side by side at the rear of a 2,2 kg heat sink, supported from a common thermal hub. The flight "standard digital watt" derives from a precision voltage and a Pulse-Width-Modulator. This PWM system has a power non-linearity < 6 ppm and eliminates the square root in the traditional servo loop.

We determine the irradiance from the real part of the sinusoidal component at the shutter frequency. This phase sensitive detection simplifies the characterisation and generates only second order effects due to timing and equivalence uncertainties. We calibrate the aperture transmission integral over area against a chrome-on-quartz ruling, transferring by CCD images. Measuring with a ½° beam through the field-of-view aperture, we determine this transmission in context. In flight, we re-characterize the servo loop gain, pointing variations, and the dark signal. We determine the equivalence ratio from models constrained by distributions and transfer functions measured by laser illumination of the cones.

## 1. Total Irradiance Monitor TIM

TIM is the Total Irradiance Monitor, one of four instruments on NASA's Earth Observing System (EOS) SOlar Radiation and Climate Experiment (SORCE). To be launched in 2002, TIM will point at the Sun on orbit, and measure the total solar irradiance (TSI) to an accuracy of 100 ppm (1 $\sigma$) and with a noise level < 1 ppm each 500 seconds. TIM will be a continuation of the TSI measurements described by Willson [1], Willson and Helizon [2], and Fröhlich et al [3,4].

TIM is an ambient temperature, active cavity radiometer consisting of four side-by-side conical cavities (cones) used in active vs. reference pairs. The concept is illustrated in Fig. 1. For illustrations and animations, see http://lasp.Colorado.edu/sorce/. Select TIM.

Features of TIM include: Nickel Phosphorous (NiP) diffuse black absorber ( Johnson [5] ), two thermal low pass filters, thick cavity walls, a buried replacement heater, stainless steel low-conductance cone supports from a common hub, servo gain dominated by thermal mass, a Digital Signal Processor (DSP) in the servo loop, a duty cycle modulated digital-to-power converter, diamond electrical insulators to isolate nodes, the precision aperture in front of the field-of-view aperture, and extraction of the irradiance from the fundamental of the shutter frequency. The existing prototype demonstrates < 1 ppm noise level. Characterization to achieve 100 ppm accuracy is ongoing.

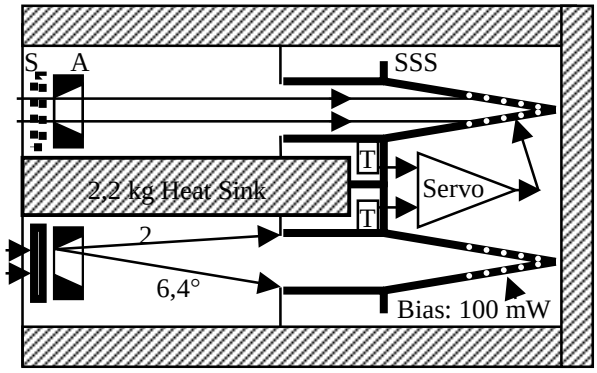


**Figure 1. Concept diagram of one of the two cavity pairs of TIM. Labeled are the shutter S, Aperture A, Stainless Steel Support SSS, and one of four thermistors T located at the support. Heater wires are imbedded in the walls of the cavities.**

## 2. Thermal Design of TIM

The cavities are electrodeposited silver with a nickel phosphorous (NiP) black interior, a 0,64 mm thick wall with gold on the exterior. At the rear of the cavity is a 10° half-angle cone, 44 mm long; and the front is a cylindrical extension 15 mm in diameter and 24,5 mm long. Four stainless steel spokes support the cavity at its center of gravity, allowing a 7°C temperature rise with the operating bias power of 100 mw. Four servo-balance thermistors are placed at the mechanical support. The four cavities cantilever from a central hub, which attenuates the effect of lateral gradients in the 2,4 kg heat sink. The flight standard resistor is the replacement heater, wound on the back of the cone with polyimide-insulated resistance wire (75Ni, 20Cr, 2.5Al, 2.5Cu). To embed the heaters inside the cavity walls, the heaters are wound at constant tension into grooves at the outside back half of the cone, vacuum encapsulated with thin epoxy, then over-plated with silver and gold. In thermal cycling tests, these resistors have shown < 5 ppm hysteresis and a TCR of 15 ppm/°C. The heat sink is made of gold plated aluminum.

To facilitate laboratory testing and to prevent contamination, the outer case of the TIM is a sealed housing with a one-time door to be opened on orbit. This outer case and the internal heat sink provide two stages of low-pass filtering against thermal noise. The DSP gently regulates the cone temperatures through the heat sink to maintain the ideal operating temperature. To design the servo system, we require an approximate model of the thermal circuits at frequencies from 0 to 50 Hz. The measurement of high accuracy radiance, however, requires precise characterisation of the thermal circuits at the shutter frequency of 10 mHz. Some relevant frequencies of TIM are: bridge and servo 100 Hz, servo closed loop band width 1 Hz, shutter 10 mHz, orbit 200 μHz, and heat sink low-pass corner 10 μHz.

Excess stray radiation modulated at the shutter frequency and absorbed into the heat sink produces a small (< 1 ppm) differential coupling to the cavities. Any thermal infrared (IR) radiation caused by this periodic stray power is shifted 90° by the heat sink mass and is therefore rejected by the phase sensitive detection.

## 3. TIM Optics

Laser measurements on prototype cavities indicate a reflectivity of 60±20 ppm. We are now beginning to measure the reflectance of the flight cavities.

IR emissions from the instrument can be modulated by the shutter and find their way to the cavity. The 10 mHz shutter, gold plated on the inside, is just in front of the precision aperture. With the shutter closed, the cavity views a combination of the low emissivity shutter, the heat sink, and the cavity itself. With the shutter open, the cavity views the heat sink, the Sun, and dark space. Model calculations predict a negative

1900 ppm shutter correction which can be determined from observations of dark space. There will be a slight extrapolation over temperature changes between observations of the Sun and dark space. The sensitivity to shutter temperature variations will be < 5 ppm/°C.

The precision aperture (50 $mm^2$) and the field of view pupil (182 $mm^2$) 104 mm behind it, define the field of view (FOV) for rejection of Earth-shine and IR. The slope angle is 2°, the cutoff angle is 6,4° as shown in Fig. 1. By putting the (smaller) precision aperture out front, we reduce the input of periodic power to the heat sink and the shutter IR correction. The cost, however, is about 430 ppm of diffracted energy that must be calibrated correctly.

The precision apertures must be calibrated and are the dominant uncertainty for TIM. We intend to compare our measurements with measurements made elsewhere. The aperture is not, as such, a geometrical area but rather a physical optical element whose transmission must be integrated over area. We define

$$A_P = \iint \mathcal{T}(x, y)\, dxdy \qquad (1)$$

Where $\mathcal{T}(x,y)$ is the transmission of the aperture with a ½° solar beam through the field of view aperture. The co-ordinates $x,y$ are measured in the plane of the aperture. $\mathcal{T}(x,y)$ is one, except within a few wavelengths of the edges, where diffraction and scattering cause the transmission to fluctuate and then drop to zero. Experimentally, we will measure this transmission by imaging an aperture illuminated with a simulated ½° solar beam, using the same pupil as in TIM, normalising the centre of the image to one, and integrating over the area. The imaging is done with a 16-bit CCD and a telecentric lens. The area scale is determined by imaging an interferometrically ruled Ronchi ruling with the same camera. The measurement will be done at several wavelengths and averaged over the solar spectrum. This image method has the advantage that it properly calibrates scattering by imperfect edges.

## 4. Detection at the Shutter Fundamental

The cones only vary in temperature a few mK during a shutter cycle because of their large mass and replacement power from the servo system. Therefore the system temperature vs. power relations are linear to better than 1 ppm. We can thus replace the time dependence of the temperature field or the power flow with a complex Fourier series in harmonics of the shutter fundamental. In particular, we will use the in-phase signal at the shutter fundamental to determine the irradiance. Thus, we need to characterise the radiometer to a few ppm at one frequency. All time dependent quantities in the model will be expressed as their complex amplitude vs. frequency. The advantages of this approach over the traditional time-domain algorithms include:

a) The shutter frequency can be selected for minimum system noise. The prototype shows < 1 ppm noise.
b) The time convolutions become multiplications of complex numbers, replacing convolutions over time. This makes the instrument characterisable.
c) The standard formalisms of servo loop design are all expressed in the frequency domain.
d) We can reject the out-of-phase component, mostly a first order effect. The in-phase component mostly has effects to second order.
e) The out-of-phase component is nominally zero. Though not used to determine irradiance, it provides a consistency check.

## 5. The Measurement Equation

We need a model of TIM. The signal flow diagram Fig. 2 defines a relation between the parameters of the system, the corrected solar irradiance $E_0$, and the Digital Data numbers $\boldsymbol{D}$.

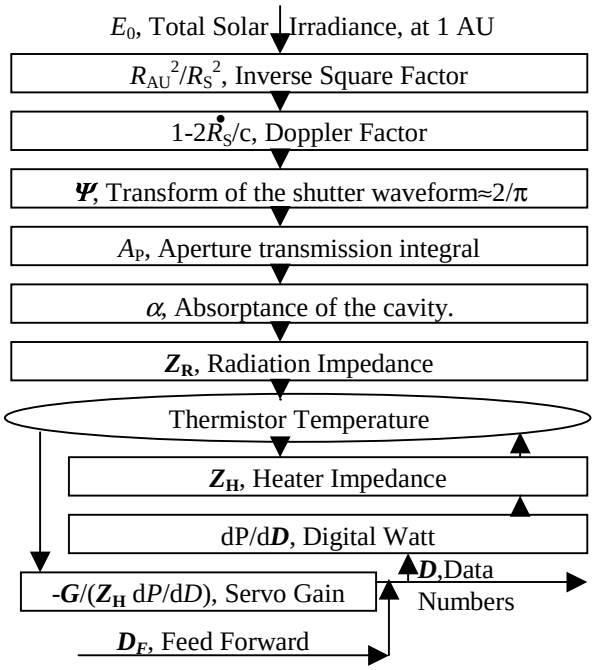


**Figure 2. Signal Flow Diagram for TIM. The arrows indicate complex number signals. The boxes are transfer functions, output/input. The bold symbols are complex numbers.**

Writing the implicit equation of Fig. 2 and solving for the irradiance gives the basic measurement equation (2).

$$E_0 = real\left\langle \frac{V^2 \quad \{-(\boldsymbol{D_S} - \boldsymbol{D_K})(1+1/\boldsymbol{G}) + \boldsymbol{D_F}/\boldsymbol{G}\}}{MR(R_0/R_S)^2(1-2\dot{R}_S/c)\boldsymbol{\Psi}\, A_P\, \alpha(\boldsymbol{Z_R}/\boldsymbol{Z_H})} \right\rangle \quad (2)$$

Where $\boldsymbol{D_S}$ are the data numbers from observations of the Sun and $\boldsymbol{D_K}$ are from observations of dark space. $\boldsymbol{G}$ is the servo loop gain at the shutter fundamental. In (2), $V$ is the standard voltage that is duty-cycle switched into the standard resistor $R$. The pulse width counter has a 100% count of $M$ = 64000 so that $D/M$ is the duty cycle of the pulses, proportional to average power. The (bold) data numbers $\boldsymbol{D}$ and the shutter transmission factor $\boldsymbol{\Psi}$ are the complex Fourier components of the observed time series at the shutter fundamental. The complex thermal impedances $\boldsymbol{Z_R}$ and $\boldsymbol{Z_H}$ are the Kelvin/Watt thermal impedances to the thermistor from the radiative input and the heater input, at the shutter fundamental.

The shutter transmission factor $\boldsymbol{\Psi}$ is very close to the ideal $2/\pi$. The shutter, with a period of 100 sec, has a delay of 20 msec and a rise time of 6 msec and a fall time of 8 msec. The actual continuous transform of this waveform is $\boldsymbol{\Psi}$ = (1 - 0,2 ppm - 1257$i$ ppm)$2/\pi$. Note that the delay causes essentially only an out-of-phase (imaginary) component.

In operation, the Data numbers $\boldsymbol{D}$ are in the spacecraft telemetry as a time series and are Fourier-analysed on the ground for application in (2). Note that the complex Fourier components in (2) occur as dimensionless ratios: $\boldsymbol{D}/\boldsymbol{\Psi}$, $\boldsymbol{Z_R}/\boldsymbol{Z_H}$, and $\boldsymbol{G}$ = ***Out***/***In***. Therefore, we can use an arbitrary but consistent normalisation of the Fourier algorithm. The time references must also be identical in numerator and denominator.

Not explicitly included in (2) are: lead resistances, lead heating, aperture temperature correction, pointing corrections, additive signals due to temperature gradients at the shutter frequency, exposure-dependent degradation, etc.

We command the feed forward signal $\boldsymbol{D_F}$ from the ground. We can set it within 1% of the expected signal, $\boldsymbol{D_S}$-$\boldsymbol{D_K}$, thereby reducing by 1/100 the uncertainties in $E_0$ due to uncertainties in the loop gain $\boldsymbol{G}$. Equivalently, we can close the shutters and calibrate $\boldsymbol{G}$ in flight using the feed forward as a test generator. We've demonstrated that this calibration can be done to <10 ppm. Since $\boldsymbol{D_F}$ is programmable, we can also use it during characterisation to measure the non-linearity of the loop.

## 6. The Equivalence Ratio, $\boldsymbol{Z_R}/\boldsymbol{Z_H}$

The thermal impedances $\boldsymbol{Z_R}$ and $\boldsymbol{Z_H}$ are the temperatures at the thermistor produced per power applied by radiation and by the replacement heater, respectively. We will determine the ratio of these thermal impedances using measurements and theory of the cavity. A heuristic, one-dimensional, analytical model will suffice here to estimate uncertainties in the equivalence ratio. Let $\varepsilon$ be the surface IR emissivity, $x$ the co-ordinate along the axis of the cavity, $D$ the cavity diffusivity, $\omega$ the shutter angular frequency, $k$ the thermal conductivity, $W$ the cavity wall thickness, $T_0$ the operating Kelvin temperature, $\sigma$ the Stefan Boltzman constant, and $\boldsymbol{U}(x,\omega)$ is the temperature field along the length of the cavity. The equation of thermal flow at frequency $\omega$ is:

$$\frac{\partial^2 \boldsymbol{U}}{\partial x^2} + \frac{1}{x}\frac{\partial \boldsymbol{U}}{\partial x} = \left(\frac{4\sigma\varepsilon T_0^3}{kW} + \frac{i\omega}{D}\right)\boldsymbol{U} \equiv -\boldsymbol{K}^2\boldsymbol{U} \quad (3)$$

Where the complex wavenumber $\boldsymbol{K}$ depends upon the shutter frequency, the diffusivity, and the ratio of radiation to conduction. Note that increasing the wall thickness lessens the effect of the distributed radiation. For our case, the radiative term is about 1000 times smaller than the diffusive term in (3). For the cylindrical extension, the first order partial derivative in (3) vanishes. The physical solutions of (3) are proportional to the Bessel functions $J_0(\boldsymbol{K}x)$ for the cone with $x$ measured from the tip and to $\mathrm{Cos}(\boldsymbol{K}x)$ for the cylindrical extension with $x$ measured from the opening. The gradients of both these solutions are zero at the ends.

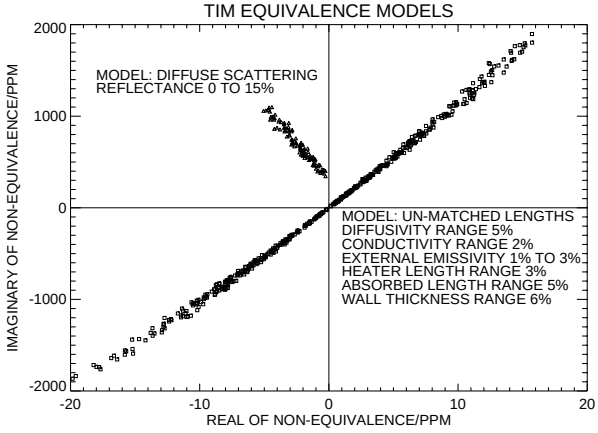


**Figure 3. Monte Carlo estimates of the non-equivalence $\ln(\boldsymbol{Z_R}/\boldsymbol{Z_H})$ given estimated uncertainties of the parameters. The uncertainty of the real part contributes to the uncertainty in the measurement.**

To obtain the equivalence ratio from the thermal solution, we need the normalised distribution of radiation $f_R(x)$ and the normalised distribution of applied heater power $f_H(x)$. Neglecting here the bounce of radiation to the front cylindrical extension, the equivalence ratio becomes:

$$\boldsymbol{Z_R}/\boldsymbol{Z_H} = \int J_0(\boldsymbol{K}x) f_R(x)\, dx \Big/ \int J_0(\boldsymbol{K}x) f_H(x)\, dx \quad (4)$$

The ratio (4) is nearly one because the two distributions are approximately the same, $\boldsymbol{K}x$ is small, and because $J_0$ has zero slope at $\boldsymbol{K}x = 0$. Two numerical examples of (4) are shown in Fig. 3.

The diffuse scattering model varies mostly with the reflectivity of the NiP black inside the cavity. The unmatched length model depends mostly on different lengths of the distributions. In both models the real part of the non-equivalence correction is < 20 ppm.

To characterise the non-equivalence, we will measure the variation of relative equivalence vs. shutter frequency. We will measure the distribution of radiation with pulsed lasers and cavities instrumented with arrays of thermistor chips. These measurements, at several wavelengths, will constrain the theoretical calculations. The effect of IR radiation inside the cone will be added as a perturbation.

## 7. Pulse Width Digital-to-Power Converter

The flight standard voltage is based on the Linear Technology LTZ1000A, a thermostatted buried zener diode. Spreadbury [6] has shown the long term stability to be better than 3 ppm/year and Rax et al [7] have studied the radiation stability of this device. There are three such references in TIM.

This precision voltage is pulse-modulated onto the standard resistors through a MOSFET switch having $R_{DSON}$ = 4 mΩ (8 ppm). Leads and traces in the system require ≈ 100 ppm corrections.

To make long term corrections, we will maintain ground witnesses of the standard resistances, voltages, apertures, and an entire instrument.

## 8. Uncertainty Budget

To estimate the accuracy of TIM, we propagate realistic parameters, with uncertainties, through the measurement equation as for example in Fig. 3. We have set ourselves a characterisation budget for each of the factors of (2) as follows: $\delta Doppler$ < 5 ppm, $\delta Inverse\ Square$ < 5 ppm, $\delta\boldsymbol{\Psi}$ < 2 ppm $\delta A_P$ < 60 ppm, $\delta\alpha$ < 20 ppm, $\delta\boldsymbol{G}$ < 5 ppm, $\delta(\boldsymbol{Z_R}/\boldsymbol{Z_H})$ < 20 ppm, $\delta V$ < 10 ppm, $\delta leads$ < 10 ppm, and $\delta R$<10 ppm. The root sum square of these uncertainties is 71 ppm. We have yet to incorporate the uncertainties due to corrections for degradation, scattered light, and pointing. We are, at this writing, most concerned about the uncertainty in the aperture.

References

1. Willson, R.C., R. S. Helizon, *Proc. of SPIE Earth Observing Systems IV Conference, Denver, CO*, 1999, **3750**, 233-242.
2. Willson, R.C., *Science*, 1997, **277**, 1963-1965.
3. Fröhlich C., Andersen B. N., Appourchaux T., Berthomieu G., Crommelynck D. A. Domingo V., Fichot A. Finsterle M.F., Gómez M. F., Gough D., Jiménez, Leifsen T., , Lombaerts M., Pap J.M., Provost J., Roca Cortés T., Romero J., Roth H., Sekii T., TellJohann U., Toutain T., and Wehrli C., In *The First Results from SOHO* Edited by B. Fleck and Z. Svestka, Dordrect /Boston /London, Kluwer Academic Publishers, 1997.pp 1-25. See also *Solar Physics*, 1997, **170** and **175.**
4. Fröhlich C., Crommelynck D.A., Wehrli C., Anklin M., Dewitte S., Fichot A., Finsterle W., Jiméniz A. Chevalier A., Roth H., In *The First Results from SOHO* Edited by B. Fleck and Z. Svestka, Dordrect /Boston /London, Kluwer Academic Publishers, 1997, 267-286. See also *Solar Physics*, 1997, **170** and **175**.
5. Johnson, C. E., *Metal Finishing*, July 1980, 22-24.
6. Spreadbury, P.J., *IEEE Trans. Instrumentation and Measurement*, **40**, 1991, 343-346.
7. Rax, B.G., Lee, C.I., and Johnston, A.H., *IEEE Trans. Nuclear Science*, **44**, 1997, 1939-1944.

Figure Captions

Figure 1. Concept diagram of one of the two cavity pairs of TIM. Labeled are the shutter S, Aperture A, Stainless Steel Support SSS, and one of four thermistors T located at the support. Heater wires are imbedded in the walls of the cavities.

Figure 2. Signal Flow Diagram for TIM. The arrows indicate complex number signals. The boxes are transfer functions, output/input. The bold symbols are complex numbers.

Figure 3. Monte Carlo estimates of the non-equivalence $\ln(\mathbf{Z_R}/\mathbf{Z_H})$ given estimated uncertainties of the parameters. The real part determines the uncertainty in the irradiance.

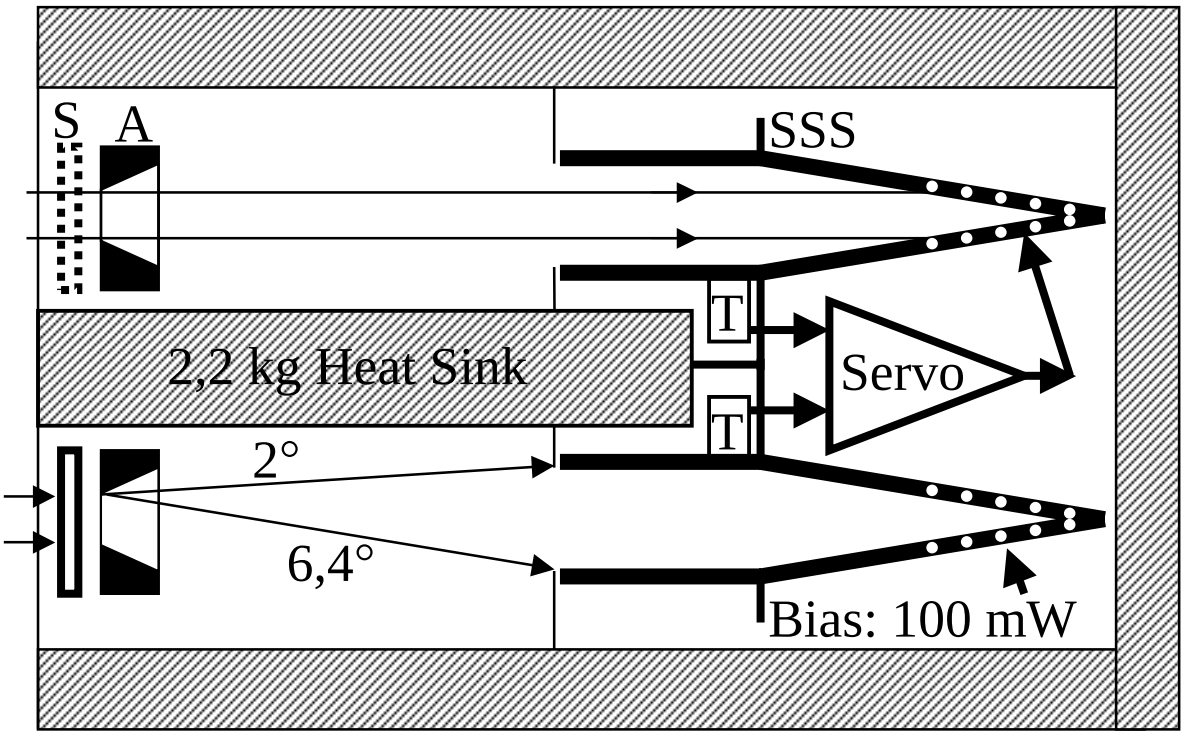


**Fig. 1, Lawrence et al.**

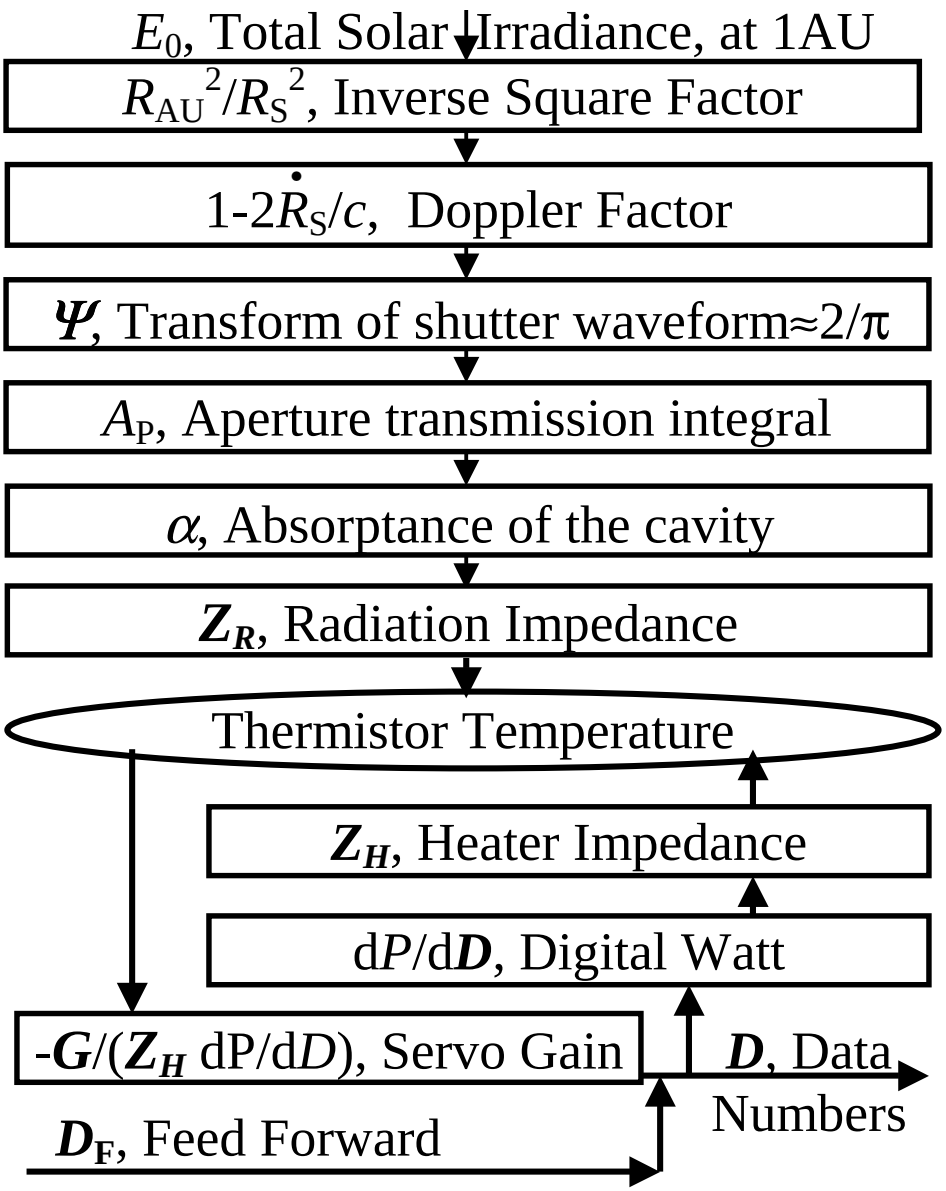


**Figure 2. Lawrence, et al**

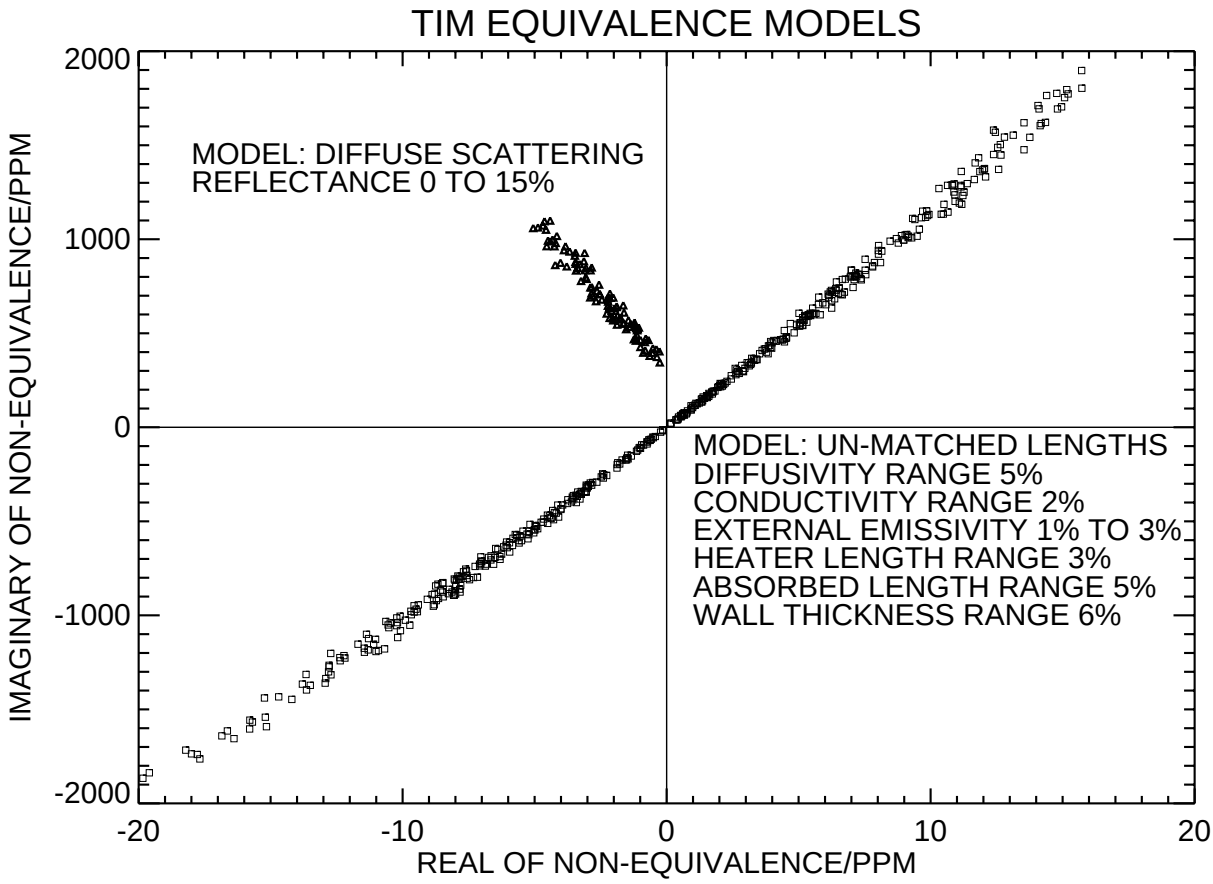


**Fig. 3. Lawrence et al.**